

Neuromorphic Processing: A Unifying Tutorial

Hamid Soleimani and Emmanuel. M. Drakakis

Abstract

All systolic or distributed neuromorphic architectures require power efficient processing nodes. In this paper, a unifying tutorial is presented which implements multiple neuromorphic processing elements using a systematic analog approach including synapse, neuron and astrocyte models. It is shown that the proposed approach can successfully synthesize multidimensional dynamical systems into analog circuitry with minimum effort.

1 Introduction

Given the application of the neuromorphic circuits, different approaches have been devised so far to mimic the biological behavior of the nervous system including special purpose computing architectures [1–5], digital [6–15], and analog platforms [16–24]. Although all these approaches have their own merits and purposes, the interest upon mimicking biological behavior in their natural form (analog) has always been pursued rigorously by researchers.

To this end, in this paper we apply a novel approach introduced in [25] to systematically synthesize different neuromorphic processing elements into CMOS circuitry operating in strong-inversion. Same approach has been applied to log-domain circuits presented in [16] with the purpose of achieving ultra-low power circuitry at the expense of slower time scales. In this tutorial, the application of the method is verified by synthesizing three different neuromorphic processing elements including synapse, neuron, and astrocyte models.

2 Method

In this section, the novel approach proposed in [25] is described which supports a systematic realization procedure of strong-inversion circuits capable of computing bilateral dynamical systems at higher speed compared to the previously proposed log-domain circuit [16]. The current relationship of an NMOS and PMOS transistor operating in strong-inversion saturation when $|V_{DS}| > |V_{GS}| - |V_{th}|$ can be expressed as follows:

$$I_{D_n} = \frac{1}{2} \mu_n C_{ox} \left(\frac{W}{L}\right)_n (V_{GS} - V_{th})^2 \quad (1)$$

$$I_{D_p} = \frac{1}{2} \mu_p C_{ox} \left(\frac{W}{L}\right)_p (V_{SG} - V_{th})^2 \quad (2)$$

where μ_n and μ_p are the charge-carrier effective mobility for NMOS and PMOS transistors, respectively; W is the gate width, L is the gate length, C_{ox} is the gate oxide capacitance per unit area and V_{th} is the threshold voltage of the device.

Setting $k_n = \frac{1}{2} \mu_n C_{ox} \left(\frac{W}{L}\right)_n$ and $k_p = \frac{1}{2} \mu_p C_{ox} \left(\frac{W}{L}\right)_p$ in (1) and (2) and differentiating with respect to time, the current expression for I_A (see Figure 1) yields:

$$\dot{I}_A = \overbrace{2k_n(V_{GS} - V_{th})}^{\sqrt{k_n I_A}} \dot{V}_{GS_1} \quad (3)$$

$$\dot{I}_A = \overbrace{2k_p(V_{SG} - V_{th})}^{\sqrt{k_p I_A}} \dot{V}_{SG_2} \quad (4)$$

(3) and (4) are equal, therefore:

$$\dot{V}_{SG_2} = \sqrt{\frac{k_n}{k_p}} \dot{V}_{GS_1} = \beta \dot{V}_{GS_1} \quad (5)$$

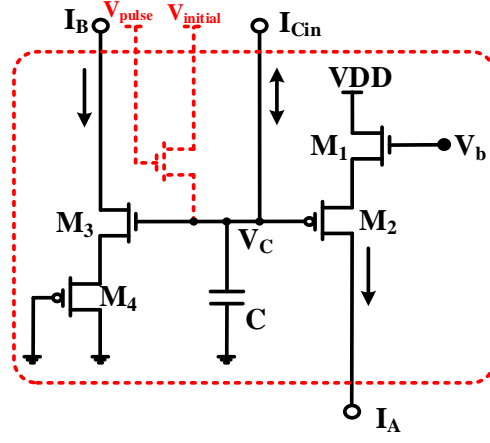


Figure 1: The “main core” including the initialization circuit highlighted with red color.

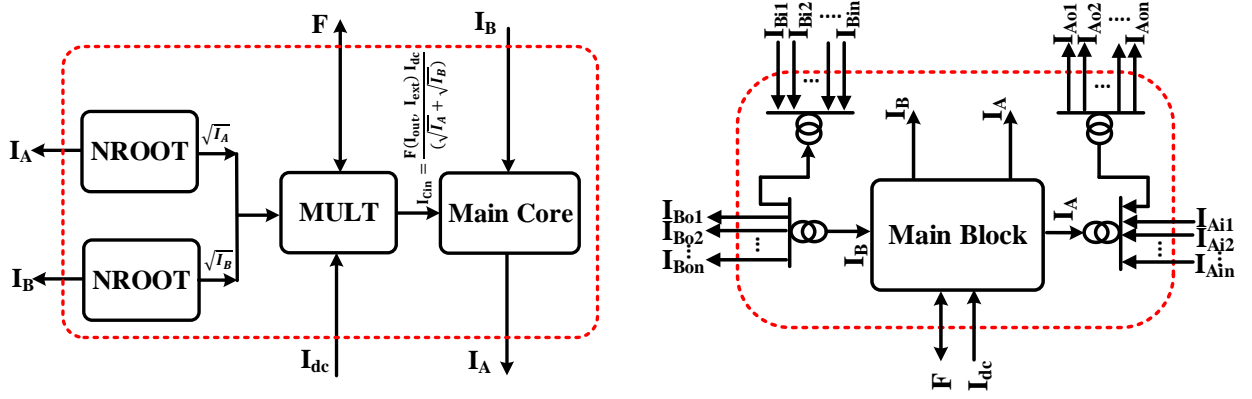


Figure 2: (a) The “main block” including the main core and two current–mode root square blocks and a bilateral multiplier. (b) The final high speed circuit including the “main block” with several copied currents (the current mirrors are represented with double circle symbols)

where $\beta = \sqrt{\frac{k_n}{k_p}}$. Similarly, we can derive the following equation for transistors M_3 and M_4 :

$$\dot{V}_{SG_4} = \sqrt{\frac{k_n}{k_p}} \dot{V}_{GS_3} = \beta \dot{V}_{GS_3}. \quad (6)$$

The application of Kirchoff’s Voltage Law (KVL) and applying the derivative function show the following relations:

$$\dot{V}_C = -(\dot{V}_{GS_1} + \dot{V}_{GS_2}) \quad (7)$$

$$\dot{V}_C = +(\dot{V}_{GS_3} + \dot{V}_{GS_4}) \quad (8)$$

where V_C is the capacitor voltage and V_b the bias voltage which is constant (see Figure 1). Substituting (5) and (6) into (7) and (8) respectively yields:

$$\dot{V}_C = -\dot{V}_{GS_1} \cdot (1 + \beta) \quad (9)$$

$$\dot{V}_C = +\dot{V}_{GS_3} \cdot (1 + \beta). \quad (10)$$

Setting the current $I_{out} = I_B - I_A$ in Figure 1 as the state variable of our system and using (3) and the corresponding equation for I_B , the following relation is derived:

$$\dot{I}_{out} = \dot{I}_B - \dot{I}_A = 2\sqrt{k_n I_B} \dot{V}_{GS_3} - 2\sqrt{k_p I_A} \dot{V}_{GS_1} \quad (11)$$

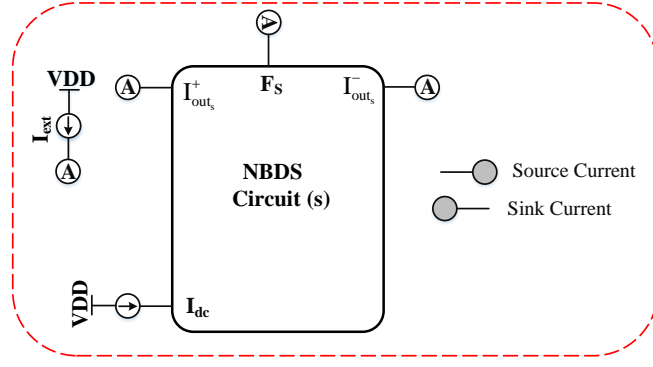


Figure 3: A block representation of the total circuit implementing the synapse model.

by substituting (9) and (10) in (11):

$$\dot{I}_{out} = (\sqrt{I_A} + \sqrt{I_B}) \cdot \frac{2\sqrt{k_n}\dot{V}_C}{2 + \beta}. \quad (12)$$

Bearing in mind that the capacitor current I_{Cin} can be expressed as $C\dot{V}_C$, relation (12) yields:

$$\dot{I}_{out} = (\sqrt{I_A} + \sqrt{I_B}) \cdot \frac{2\sqrt{k_n}I_{Cin}}{(2 + \beta)C}. \quad (13)$$

One can show that:

$$\frac{(2 + \beta)C}{2\sqrt{k_n} \cdot I_{dc}} \dot{I}_{out} = \frac{(\sqrt{I_A} + \sqrt{I_B})}{I_{dc}} \cdot I_{Cin}. \quad (14)$$

Equation (14) is the main core's relation. In order for a high speed mathematical dynamical system with the following general form to be mapped to (14):

$$\tau \dot{I}_{out} = F(I_{out}, I_{ext}) \quad (15)$$

where I_{ext} and I_{out} are the external and state variable currents, the quantities $\frac{C}{I_{dc}}$ and I_{Cin} must be respectively equal to $\frac{2\tau\sqrt{k_n}}{(2+\beta)}$ and $\frac{F(I_{out}, I_{ext})I_{dc}}{(\sqrt{I_A} + \sqrt{I_B})}$. Note that the ratio value $\frac{C}{I_{dc}}$ can be satisfied with different individual values for C and I_{dc} . These values should be chosen appropriately according to practical considerations (see Section V.G). Since F is a bilateral function, in general, it will hold:

$$I_{Cin} = \frac{\overbrace{F^+(I_A, I_B, I_{ext}^+, I_{ext}^-)I_{dc}}^{I_{Cin}^+}}{(\sqrt{I_A} + \sqrt{I_B})} - \frac{\overbrace{F^-(I_A, I_B, I_{ext}^+, I_{ext}^-)I_{dc}}^{I_{Cin}^-}}{(\sqrt{I_A} + \sqrt{I_B})} \quad (16)$$

where I_{Cin}^+ and I_{Cin}^- are calculated respectively by a root square block (see Figure 2(a) and I_{ext} is separated to + and - signals by means of splitter blocks. Note that I_{dc} is a scaling dc current and τ has dimensions of *second(s)*. Since I_{Cin} can be a complicated nonlinear function in dynamical systems, we need to provide copies of I_{out} or equivalently of I_A and I_B to simplify the systematic computation at the circuit level. Therefore, the higher hierarchical block shown in Figure 2(b) is defined as the NBDS (Nonlinear Bilateral Dynamical System) circuit [16] (see Figure 2(b)) including the main block and associated current mirrors. The form of (15) is extracted for a 1-D dynamical system and can be extended to N dimensions in a straightforward manner as follows:

$$\tau_N \dot{I}_{out_N} = F_N(\bar{I}_{out}, \bar{I}_{ext}) \quad (17)$$

where $\frac{C_N}{I_{dcN}} = \frac{2\tau_N\sqrt{k_n}}{(2+\beta)}$ and $I_{Cin_N} = \frac{F_N(\bar{I}_{out}, \bar{I}_{ext})I_{dcN}}{(\sqrt{I_{A_N}} + \sqrt{I_{B_N}})}$.

To realized the full potential of 17 and implement the aforementioned neuromorphic processing elements, some circuit blocks are required to perform basic operations including multiplication and division. The full description of these blocks can be found in [25], however, in this paper we only employ them to implement the following case studies. In the following sections, multiple neuromorphic processing elements are implemented in which the feasibility of the above method is shown.

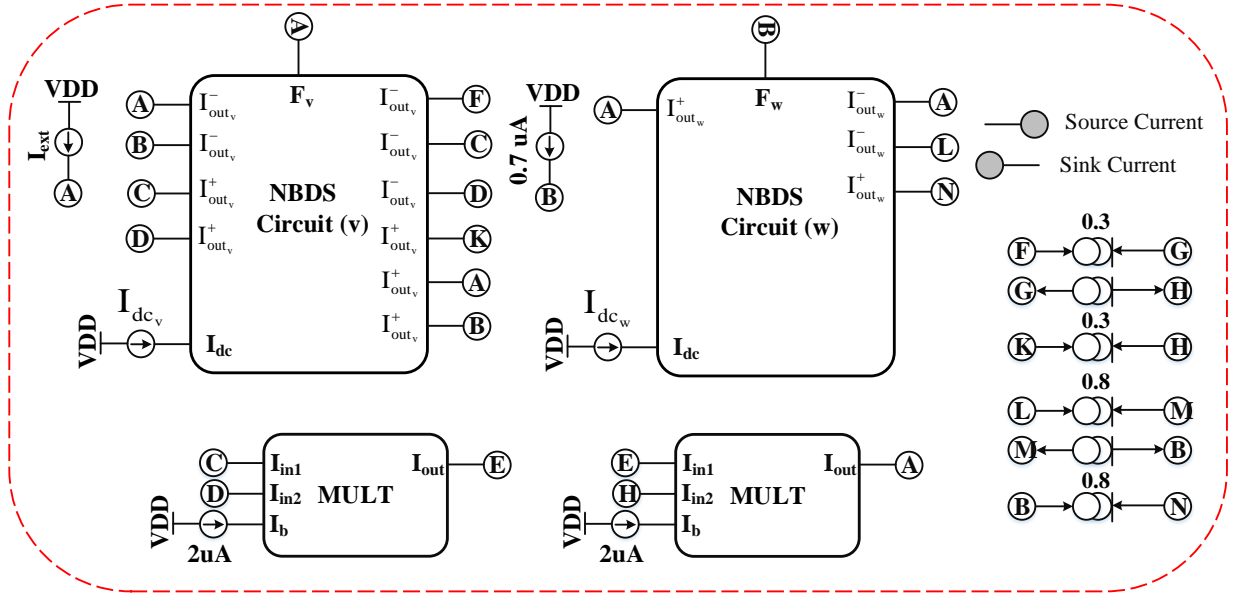


Figure 4: A block representation of the total circuit implementing the 2-D FHN neuron model.

2.1 Synapse model

Synapses can be represented as low pass filters as the conductance and the capacitance of the post-synaptic cell are connected in parallel, forming a circuit in which the membrane's capacitance takes time to charge. Therefore they function as low-pass filters attenuating the high frequency components of a pre-synaptic signals. The filtering characteristics including the time scale of a synapse can vary depending upon the membrane properties of the post-synaptic cell. Low pass filters can be generally represented as:

$$\tau \dot{s} = -s + I_{ext} \quad (18)$$

where τ defines the response time scale of the synapse. We can start forming the electrical equivalent using (17):

$$\left\{ \frac{(2+\beta)C}{2\sqrt{k_n} \cdot I_{dc_s}} \dot{I}_{out_s} = F_s(I_{out_s}, I_{ext}) \right. \quad (19)$$

where $I_{dc} = I_{dc_s}$, F_s is function given by:

$$\left\{ F_v(I_{out_s}, I_{ext}) = -I_{out_s} + I_{ext} \right. \quad (20)$$

It should be noted that the appropriate size of the capacitor C can be defined based on the relative time scale of the model and I_{dc} . It was shown in [16] that there are some trade-offs between the size of the capacitor and I_{dc} , in terms of power, area and noise performance. Schematic diagrams for the synapse model is seen in Figure 3, including the symbolic representation of the basic electrical blocks introduced in [25]. According to these diagrams, it is observed how the mathematical model is mapped onto the proposed electrical circuit. The schematic contains only one NBDS circuit implementing the only dynamical variable and the necessary connections. As shown in the figure, according to the synapse model parameter, proper bias currents are selected and the correspondence between the biological voltage and electrical current is $V \iff uA$.

2.2 Neuron model

In this section, the application of the method is demonstrated by synthesizing the 2-D nonlinear FitzHugh-Nagumo neuron model. In the FHN neuron model [26] with the following representation:

$$\begin{cases} \dot{v} = v - \frac{v^3}{3} - w + I_{ext} \\ \dot{w} = 0.18(v + 0.7 - 0.8w) \end{cases} \quad (21)$$

describing the membrane potential's and the recovery variable's velocity. According to this biological dynamical system, we can start forming the electrical equivalent using (17):

$$\begin{cases} \frac{(2+\beta)C}{2\sqrt{k_n} \cdot I_{dc_v}} \dot{I}_{out_v} = F_v(I_{out_v}, I_{out_w}, I_{ext}) \\ \frac{(2+\beta)C}{2\sqrt{k_n} \cdot I_{dc_w}} \dot{I}_{out_w} = F_w(I_{out_v}, I_{out_w}) \end{cases} \quad (22)$$

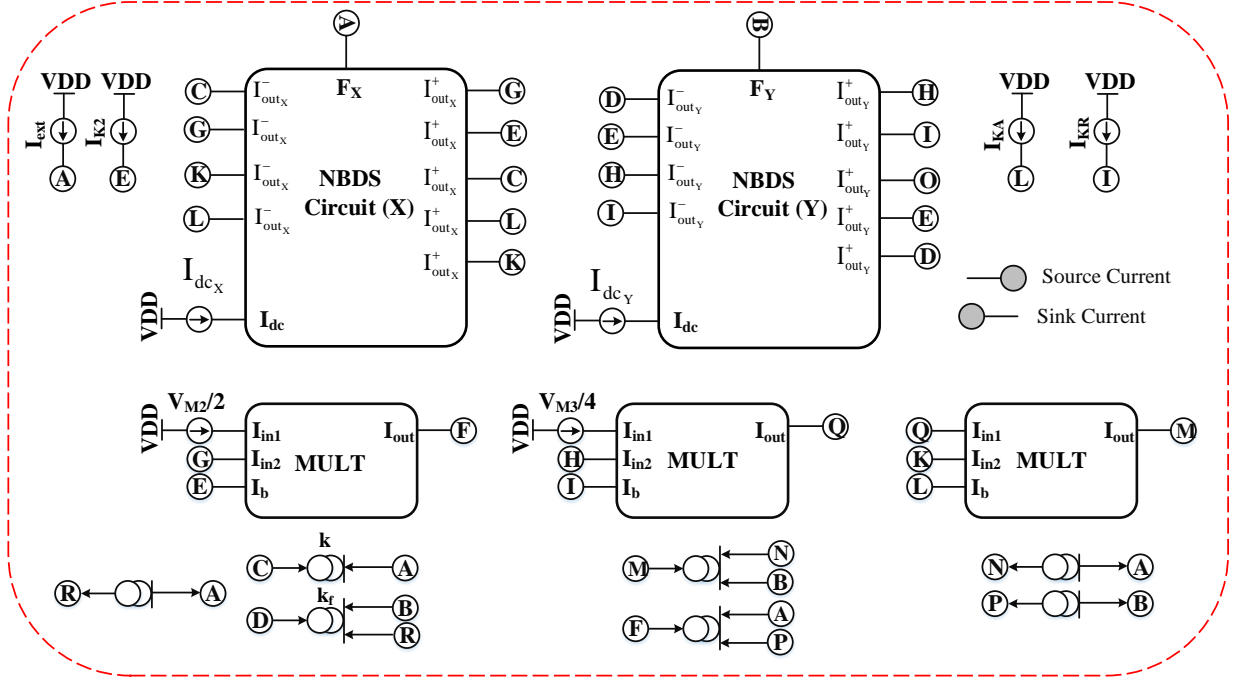


Figure 5: A block representation of the total circuit implementing the astrocyte model.

where $\tau_v = 0.18\tau_w$, and $I_{dc_v} = 0.18I_{dc_w}$, F_v and F_w are functions given by:

$$\begin{cases} F_v(I_{out_v}, I_{out_w}, I_{ext}) = I_{out_v} - \frac{I_{out_v}^3}{I_b I_x} - I_{out_w} + I_{ext} \\ F_w(I_{out_v}, I_{out_w}) = (I_{out_v} + I_c - \frac{I_d I_{out_w}}{I_x}). \end{cases} \quad (23)$$

It should be noted that the appropriate size of the capacitor C can be defined based on the relative time scale of the model. Schematic diagrams for the FHN neuron model is seen in Figure 4, including the symbolic representation of the basic blocks introduced in [25]. According to these diagrams, it is observed how the mathematical model is mapped onto the proposed electrical circuit. The schematic contains two NBDS circuits implementing the two dynamical variables, followed by two MULT blocks and current mirrors realizing the dynamical functions. As shown in the figure, according to the neuron model, proper bias currents are selected and the correspondence between the biological voltage and electrical current is $V \iff uA$.

2.3 Astrocyte model

Astrocytes are part of the biological neural network that outnumber neurons by over a factor of five in the brain. They occur in the entire central nervous system (CNS) and perform many essential complex functions in the healthy CNS [27]. A reduced and an extended model, which accurately and efficiently describe Ca^{2+} oscillations was presented in [28]. Relying on the fact that the amount of Ca^{2+} released is controlled by the level of stimulus through modulation of the IP_3 level and by making the simplification that the level of stimulus-induced, IP_3 -mediated Ca^{2+} is a model parameter, the following 2-D model was presented:

$$\begin{cases} \dot{X} = z_0 + z_1\beta - z_2(X) + z_3(X, Y) + k_f Y - kX \\ \dot{Y} = z_2(X) - z_3(X, Y) - k_f Y \end{cases} \quad (24)$$

where

$$\begin{cases} z_2(X) = V_{M_2} \frac{X^n}{K_2^n + X^n} \\ z_3(X, Y) = V_{M_3} \frac{Y^m}{K_R^m + Y^m} \frac{X^p}{K_A^p + X^p} \end{cases} \quad (25)$$

The parameters V_{M_2} , V_{M_3} , K_2 , K_R , K_A , k_f and k are the maximum values of z_2 and z_3 , threshold constants for pumping, release and activation and rate constants, respectively. Parameters n , m , and p define the Hill coefficients characterizing the pumping, release and activation processes, respectively. Depending on the values of the Hill coefficients, different degrees of cooperativity can be achieved. There are three different cases of Hill coefficients ($m = n = p = 1$, $m = n = p = 2$ and $m = n = 2, p = 4$) which in this paper we only explore the $m = n = p = 1$ case and leave the rest to the interested readers. The electrical equivalent can be represented

as follows:

$$\begin{cases} \frac{(2+\beta)C}{2\sqrt{k_n \cdot I_{dcX}}} \dot{I}_{outX} = F_X(I_{outX}, I_{outY}, I_{ext}) \\ \frac{(2+\beta)C}{2\sqrt{k_n \cdot I_{dcY}}} \dot{I}_{outY} = F_Y(I_{outX}, I_{outY}) \end{cases} \quad (26)$$

where $I_{ext} = z_0 + z_1\beta$, F_X and F_Y are functions given by:

$$\begin{cases} F_X(I_{outX}, I_{outY}, I_{ext}) = -\frac{I_{VM2} I_{outX}}{I_{K2} + I_{outX}} + \frac{I_{VM3} I_{outY}}{I_{KR} + I_{outY}} \frac{I_{outX}}{I_{KA} + I_{outX}} - k I_{outX} + k_f I_{outY} + I_{ext} \\ F_Y(I_{outX}, I_{outY}) = \frac{I_{VM2} I_{outX}}{I_{K2} + I_{outX}} - \frac{I_{VM3} I_{outY}}{I_{KR} + I_{outY}} \frac{I_{outX}}{I_{KA} + I_{outX}} - k_f I_{outY}. \end{cases} \quad (27)$$

It should be noted that the appropriate size of the capacitor C can be defined based on the relative time scale of the model. Schematic diagrams for the Astrocyte Ca^{2+} oscillations model is seen in Figure 5, including the symbolic representation of the basic blocks introduced in [25]. According to these diagrams, it is observed how the mathematical model is mapped onto the proposed electrical circuit. The schematic contains two NBDS circuits implementing the two dynamical variables, followed by three MULT blocks and current mirrors realizing the dynamical functions. As shown in the figure, according to the neuron model, proper bias currents are selected and the correspondence between the biological voltage and electrical current is $V \iff uA$.

3 Discussion

In this paper, we demonstrated a unifying tutorial which synthesizes biological neuromorphic models into analog circuitry with the minimum effort. The validity of the approach was shown by implementing multiple neuromorphic processing elements including synapse, neuron and astrocyte models. As mentioned above there are multiple design trade-off aspects (including but not limited to the capacitor sizes and bias currents (I_{dc})) that interested readers should be aware of in order to design a power efficient circuitry.

References

- [1] S B Furber, F Galluppi, S Temple, and L A Plana. The spinnaker project. *Proceedings of the IEEE*, 102(5):652–665, 2014.
- [2] H Soleimani and A Ahmadi. A gpu based simulation of multilayer spiking neural networks. In *19th Iranian Conference on Electrical Engineering*, pages 1–5. IEEE, 2011.
- [3] Tesla k80 gpu accelerator. *Board Specification* <https://images.nvidia.com/content/pdf/kepler/Tesla-K80-BoardSpec-07317-001-v05.pdf>, 2015.
- [4] Intel xeon processor e5–4669 v3. <http://ark.intel.com/products/85766/Intel-Xeon-Processor-E5-4669-v3-45M-Cache-2.10-GHz>, 2016.
- [5] J M Nageswaran, N Dutt, J L Krichmar, A Nicolau, and A V Veidenbaum. A configurable simulation environment for the efficient simulation of large-scale spiking neural networks on graphics processors. *Neural networks*, 22(5):791–800, 2009.
- [6] H Soleimani and M Drakakis, E. A low–power digital ic emulating intracellular calcium dynamics. *International Journal of Circuit Theory and Applications*, 46(11):1929–1939, 2018.
- [7] H Soleimani and M Drakakis, E. An efficient and reconfigurable synchronous neuron model. *IEEE Transactions on Circuits and Systems II: Express Briefs*, 65(1):91–95, 2017.
- [8] T Matsubara and Torikai. Asynchronous cellular automaton-based neuron: theoretical analysis and on-fpga learning. *IEEE transactions on neural networks and learning systems*, 24(5):736–748, 2013.
- [9] A Cassidy and A G Andreou. Dynamical digital silicon neurons. *IEEE Biomedical Circuits and Systems Conference*, pages 289–292, 2008.
- [10] T Hishiki and H Torikai. A novel rotate-and-fire digital spiking neuron and its neuron-like bifurcations and responses. *Neural Networks and Learning Systems, IEEE Transactions on*, 22(5):752–767, 2011.
- [11] H Soleimani, A Ahmadi, and M Bavandpour. Biologically inspired spiking neurons: Piecewise linear models and digital implementation. *Circuit and System I Regular Paper, IEEE Transactions on*, 59(12):2991–3004, 2012.

- [12] H Soleimani, M Bavandpour, A Ahmadi, and D Abbott. Digital implementation of a biological astrocyte model and its application. *IEEE Trans. Neural Netw. Learn. Syst.*, 26(1):127–139, 2015.
- [13] H Soleimani and E M Drakakis. A compact synchronous cellular model of nonlinear calcium dynamics: simulation and fpga synthesis results. *IEEE Trans. Biomedical Circuit and Systems*, 17(3):703–713, 2017.
- [14] E Jokar and H Soleimani. Digital multiplierless realization of a calcium-based plasticity model. *IEEE Transactions on Circuits and Systems II: Express Briefs*, 64(7):832–836, 2016.
- [15] A Makhlooghpour, H Soleimani, A Ahmadi, M Zwolinski, and M Saif. High accuracy implementation of adaptive exponential integrated and fire neuron model. In *2016 International Joint Conference on Neural Networks (IJCNN)*, pages 192–197. IEEE, 2016.
- [16] E Jokar, H Soleimani, and M Drakakis, E. Systematic computation of nonlinear bilateral dynamical systems with a novel low-power log-domain circuit. *IEEE Transactions on Circuits and Systems I: Regular Papers*, 64(8):2013 – 2025, 2017.
- [17] S S Woo, J Kim, and R Sarpeshkar. A cytomorphic chip for quantitative modeling of fundamental biomolecular circuits. *Biomedical Circuits and Systems, IEEE Transactions on*, 9(4):527–542, 2015.
- [18] G Indiveri, E Chicca, and R Douglas. A vlsi array of low-power spiking neurons and bistable synapses with spike-timing dependent plasticity. *Neural Networks, IEEE Transactions on*, 17(1):211–221, 2006.
- [19] A Houssein, K I Papadimitriou, and E M Drakakis. A 1.26 μ w cytomimetic ic emulating complex nonlinear mammalian cell cycle dynamics: Synthesis, simulation and proof-of-concept measured results. *Biomedical Circuits and Systems, IEEE Transactions on*, 9(4):543–554, 2015.
- [20] K I Papadimitriou, G B V Stan, and E M Drakakis. Systematic computation of nonlinear cellular and molecular dynamics with low-power cytomimetic circuits: a simulation study. *PloS one*, 8(2):e53591, 2013.
- [21] S Moradi and G Indiveri. An event-based neural network architecture with an asynchronous programmable synaptic memory. *Biomedical Circuits and Systems, IEEE Transactions on*, 8(1):98–107, 2014.
- [22] M Bavandpour, H Soleimani, S Bagheri-Shouraki, A Ahmadi, D Abbott, and L O Chua. Cellular memristive dynamical systems (cmds). *International Journal of Bifurcation and Chaos*, 24(5):1430016–1–1430016–22, 2014.
- [23] M Bavandpour, H Soleimani, B Linares-Barranco, D Abbott, and L O Chua. Generalized reconfigurable memristive dynamical system (mds) for neuromorphic applications. *Frontiers in neuroscience*, 9(409):1–19, 2015.
- [24] H Soleimani, A Ahmadi, M Bavandpour, and O Sharifipoor. A generalized analog implementation of piecewise linear neuron models using ccii building blocks. *Neural Networks*, 51:26–38, 2014.
- [25] H Soleimani and M Drakakis, E. A generalized strong-inversion cmos circuitry for neuromorphic applications. *arXiv preprint arXiv:2007.13941*, 2020.
- [26] R FitzHugh. Impulses and physiological states in theoretical models of nerve membrane. *J. Biophys.*, 1(6):445–466, 1961.
- [27] M V Sofroniew and H V Vinters. Astrocytes: biology and pathology. *Acta neuropathologica*, 119(1):7–35, 2010.
- [28] D Dupont and A Goldbeter. Astrocytes: biology and pathology. *Cell Calcium*, 14(4):311–322, 1993.